Research Report

Pyridyl Ligand-bridged Mesoporous Organosilicas for Metal Complex Formation on the Pore Surfaces

Minoru Waki, Yoshifumi Maegawa, Norihiro Mizoshita, Takao Tani and Shinji Inagaki

Report received on Jan. 8, 2016

ABSTRACT The first crystal-like mesoporous organosilicas (PMOs) containing three types of pyridyl ligand: divinylpyridine (v-Py), phenylpyridine (PPy), and bipyridine (BPy), were prepared from well-designed alkoxysilane precursors, which were synthesized in appropriate routes. The formation of mesoporous and molecularly-ordered periodic structures was clearly confirmed for these PMOs. The pyridyl groups in the framework of these PMOs can act as metal coordination ligands to incorporate functional metal complexes on the pore surfaces. v-Py-PMO showed excellent copper ion adsorption properties. PPy-PMO and BPy-PMO enabled the incorporation of photochemically active metal complexes such as ruthenium (Ru) and iridium (Ir) complexes. Ir(cod)(OMe)-BPy-PMO (cod = 1,5-cyclooctadiene) exhibited high performance as a heterogeneous catalyst for iridium-catalyzed C-H borylation. Ru-BPy-PMO acted as a photosensitizer for a photocatalytic hydrogen evolution system in the presence of platinum particles on the BPy-PMO surface.

KEYWORDS Periodic Mesoporous Organosilica, Pyridine, Phenylpyridine, Bipyridine, Metal Complex, Heterogeneous Catalyst, Photocatalyst

1. Introduction

Periodic mesoporous organosilicas (PMOs) are unique hybrid materials that have been synthesized by surfactant-templated supramolecular assembly and the subsequent condensation of bis-alkoxysilylated precursor compounds bridging organic groups.[1-3] Many PMOs have been synthesized from a variety of alkoxyorganosilanes containing aliphatic and aromatic hydrocarbons.[4-6] It is important to note that some PMOs bearing benzene,[7] biphenyl,[8] ethene,[9] divinylbenzene,[10,11] and naphthalene[12] groups have molecularly-ordered periodic structures that form crystal-like pore walls. The organic groups are densely embedded within the pore walls, and are regularly aligned on the pore surfaces. This molecular-scale ordering has the potential to induce unique chemical and physical properties owing to the interactive organic groups in the PMO framework.[13,14]

Amines are functional organic group containing a nitrogen atom, and have basicity due to a lone pair. Among amines, pyridine, a heterocyclic aromatic amine, is a well-known organic base for organic synthesis and metal binding. Functionalization of mesoporous silica and organosilica by immobilizing pyridine groups can allow the introduction of metal species for applications such as heterogeneous catalysts and adsorbents.[15-17] Usually, surface modification with pyridine groups has been carried out by post-synthesis grafting or co-condensation using monosilylated organosilanes containing pyridine groups. However, there are some problems with these approaches. The grafting method causes pore blockage by organic groups and would hinder the diffusion of guest substrates into the mesochannel. The co-condensation method usually requires significant dilution of the pyridine groups with a pure silicon source such as tetraethoxysilane. So far, there have been no reports of a pyridine-containing crystal-like PMO prepared from 100% pyridylsilane precursors.

In this paper, we report the synthesis of novel crystal-like PMOs containing pyridyl ligands, divinylpyridine (v-Py),[18] phenylpyridine (PPy),[19] and bipyridine (BPy),[20] and focus on the metal coordination properties on their pore surfaces. Furthermore, we describe the application of a metal-complexed PMO as a heterogeneous catalyst for the direct C-H borylation of arenes and as a photocatalytic hydrogen evolution system.

2. Results and Discussion

2. 1 v-Py-PMO

Rhodium-catalyzed silylation is one of the most useful methods for synthesizing alkoxysilylated aromatics.[21,22] However, this silylation reaction was unsuccessful for pyridine derivatives, indicating that *N*-heterocycles are inactive for disubstitution by trialkoxysilane. As an alternative approach for the synthesis of pyridyl alkoxysilane as a PMO precursor, we succeeded in synthesizing a pyridine-derived precursor by the hydrosilylation of 2,5-diethynylpyridine, yielding 2,5-bis[(*E*)-2-(triethoxysilyl)vinyl]pyridine (**3**) (**Scheme 1**). The first v-Py-PMO was obtained by the polycondensation of **3** in the presence of a cationic template surfactant under basic conditions, followed by the removal of the surfactant by HCl/ethanol extraction.

We confirmed the preservation of the v-Py groups in the framework during the PMO synthesis by solid-state nuclear magnetic resonance (NMR) and infrared (IR) analyses. The spectra showed characteristic peaks due to the aromatic and vinylic groups of v-Py units. Elemental analysis indicated that the v-Py groups were densely and covalently embedded within the framework with the content of 3.36 mmol·g^{-1}.

Powder X-ray diffraction (XRD) analysis of v-Py-PMO (**Fig. 1**(A)) showed a characteristic intense peak due to an ordered mesostructure at 2θ = 1.88°, which corresponds to a d-spacing of 4.70 nm. In addition, a peak due to molecular-scale periodicity was observed at 7.4°, with higher order diffraction peaks at 14.8, 22.5, and 30.1° in the medium angular range, indicating a lamellar periodicity of v-Py groups with an interval of 1.16 nm in the PMO framework. Figure 1(B) shows nitrogen adsorption/desorption isotherms for v-Py-PMO. The isotherms were type IV, typical of mesoporous materials. The pore surface area, estimated using the Brunauer-Emmett-Teller method, was 803 m^{2}g^{-1}, and the pore volume was calculated to be 0.683 cm^{3}g^{-1} using a t-plot analysis. The pore size distribution obtained from DFT calculations was somewhat broad, and the mean pore diameter was 4.1 nm. A transmission electron microscopy (TEM) image and a structural model of v-Py-PMO are shown in Figs. 1(C) and (D), respectively. The TEM image indicates that the v-Py-PMO had a bundle structure with one-dimensional channels at 4-5 nm intervals. The inset image clearly shows that many lattice fringes existed in the direction perpendicular to the channels. These observations suggest that v-Py groups align their molecular axes parallel to the channel direction. The structural model in Fig. 1(D) is based on the assumption of hexagonal packing. The pore wall thickness was estimated to be 1.3 nm from the pore diameter of 4.1 nm and the mesopore periodicity of 4.7 nm. v-Py groups were embedded with lamellar periodicity at 1.16 nm intervals in the framework, which indicates the formation of a crystal-like pore wall structure.

The v-Py groups maintained their chemical functionality within the PMO framework, and protons were able to access the pyridine nitrogen in the mesochannels (**Fig. 2**). A fluorescence spectrum of v-Py-PMO showed an emission band at 390 nm (**Fig. 3**(A)). Exposure of v-Py-PMO to HCl vapor increased the emission band at 470 nm and decreased the band at 390 nm. The fluorescence band at 470 nm was assignable to protonated v-Py species, indicating that the v-Py groups in the framework were almost fully protonated (Fig. 3(A)). Subsequent exposure to ammonia vapor returned the spectrum almost to its original form (Fig. 3(A)). This indicates that the v-Py groups were reversibly protonated and deprotonated. The π-π* absorption edge for the v-Py groups in the UV/Vis spectra also showed a reversible wavelength shift during the protonation and deprotonation experiment (Fig. 3(A)).

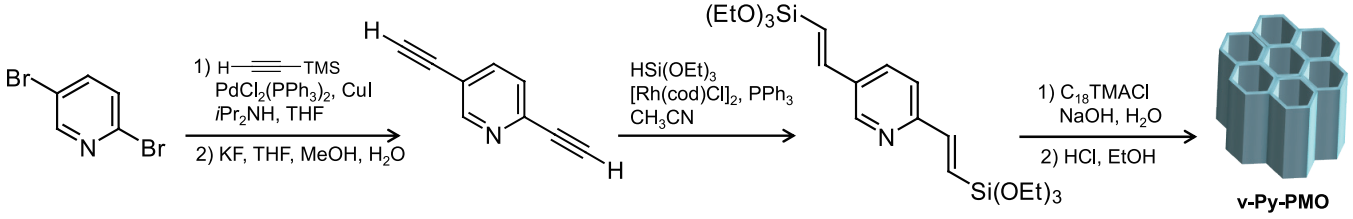

Scheme 1 Synthesis of pyridyl alkoxysilane and v-Py-PMO.

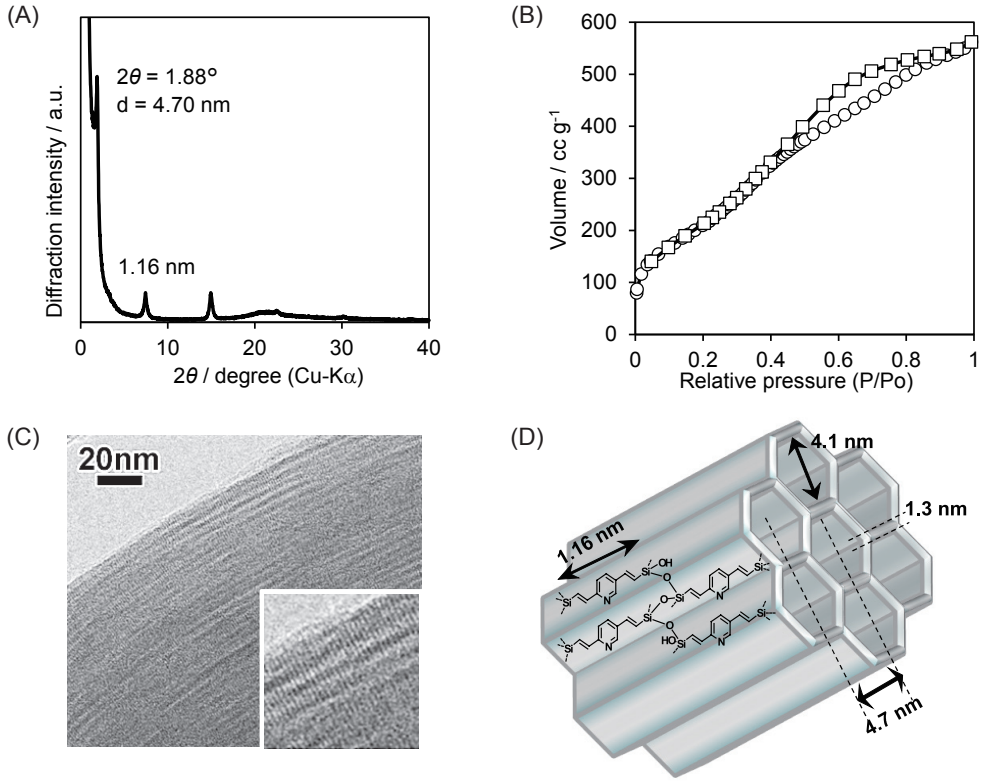

Fig. 1 (A) XRD pattern, (B) nitrogen adsorption/desorption isotherms, (C) TEM images, and (D) structural model of v-Py-PMO.

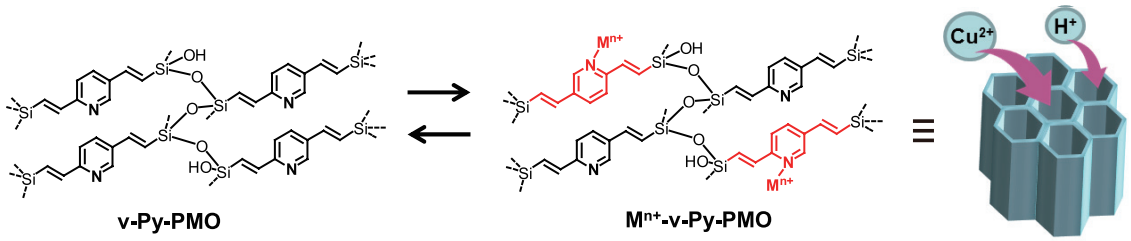

Fig. 2 Protonation and metal coordination of v-Py groups in the PMO framework.

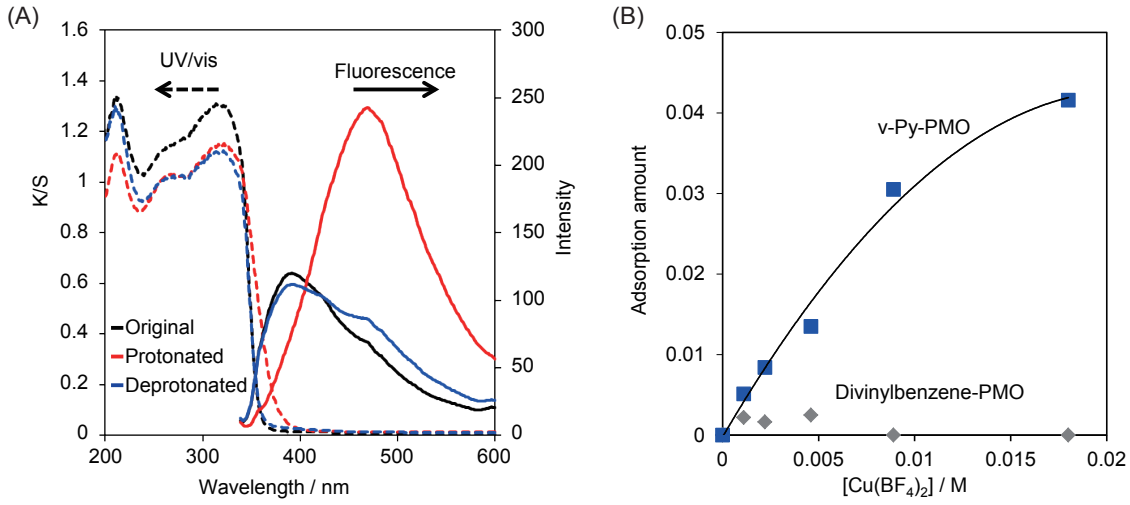

Fig. 3 (A) UV/Vis diffuse reflectance and fluorescence (λ_{ex} = 320 nm) spectra of v-Py-PMO. (B) Changes in the amount of Cu^{2+} adsorbed by v-Py-PMO. $[Cu(BF_4)_2]$ = 0-1.8 × 10^{-2} M.

The metal coordination property of v-Py-PMO was investigated by copper ion (Cu^{2+}) adsorption testing. Figure 3(B) shows the amounts of metal adsorbed on v-Py-PMO from Cu^{2+} solutions in CH_2Cl_2/MeOH. The amount increased with increasing initial $Cu(BF_4)_2$ concentration, whereas a divinylbenzene PMO with a similar molecular arrangement of the organic group showed little Cu^{2+} adsorption capacity, indicating that v-Py groups function as metal coordination sites in the PMO framework (Fig. 2).

2. 2 PPy-PMO

Ruthenium (Ru) and iridium (Ir) complexes, which are octahedral d^6 metal complexes, have received considerable attention in the field of photochemistry, including applications in organic light emitting devices,[23,24] dye-sensitized solar cells,[25] and photocatalysts.[26,27] These octahedral metal complexes usually contain bipyridine (BPy) and phenylpyridine (PPy) as typical chelating ligands. The PPy group can interact with a transition metal on a nitrogen atom as an electron donor, followed by the intramolecular activation of a C-H bond in PPy (**Scheme 2**).[28,29] This reaction is called cyclometalation, and is well known in organometallic compounds with carbon-metal σ bonds. Thus, it is important to synthesize a PMO that includes a cyclometalation PPy ligand as an organic bridge in the pore wall. Such a PMO would be advantageous for the dense and selective integration of metal complexes on the pore surface.

PPy-PMO was prepared by basic hydrolysis and polycondensation of a PPy-bis(triethoxysilane) precursor, which was synthesized from 2,5-dibromopyridine as a starting material in four steps, as shown in **Scheme 3**. The PPy-PMO material had a mesoscopically ordered porous structure with crystal-like pore walls containing a cyclometalation ligand in the framework.[19] The meso- and molecular-scale structural properties of the PPy-PMO were close to those of a previously reported biphenyl PMO.[8]

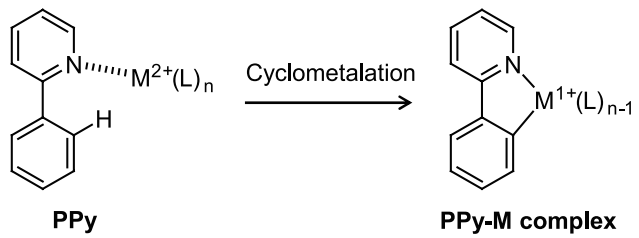

Scheme 2 Cyclometalation of a PPy ligand with transition metal ions.

The cyclometalation reaction was carried out in the presence of K_2CO_3 at 120°C by heating a solution of $[Ru(bpy)_2Cl_2]\cdot 2H_2O$ or $[Ir(ppy)_2Cl]_2$ with PPy-PMO powder (**Fig. 4**). The Ru-PPy-PMO had UV/Vis absorption peaks at 372, 416, 497, and 550 nm, in addition to the π-π* band of the PPy group at 305 nm. These peaks in the visible region can be assigned to a metal-to-ligand charge transfer (MLCT) transition. The spectral shape was very similar to that for the model complex, $[Ru^{II}(bpy)_2(ppy)]^+$ (**Figs. 5**(A) and (B)). The spectrum of Ir-PPy-PMO exhibited a broad absorption band around 380 nm, assignable to the ^{1}MLCT transition. On the other hand, the shoulder band at 480 nm corresponds to the ^{3}MLCT transition, according to the previous literature (Fig. 5(C)).[30] In the photoluminescence spectra of Ir-PPy-PMO, an emission band was observed at 550 nm with a low quantum yield of 0.03 and lifetimes of 250 ns and 1.0 μs (Fig. 5(D)).[19] Moreover, an oxygen quenching test provided evidence for phosphorescence emission from the Ir complex of Ir-PPy-PMO. These optical properties of Ir-PPy-PMO were in good agreement with those of the typical meridional isomer of the Ir complex. It is known that the meridional isomer is usually obtained when the synthesis is carried out at a lower temperature (< 140°C). Energy-dispersive X-ray spectroscopy (EDS) was used to determine the amount of metal complexes loaded into the PPy-PMO. EDS elemental analysis of Ru-PPy-PMO and Ir-PPy-PMO gave atomic ratios of Ru/PPy = 0.1 and Ir/PPy = 0.02, respectively. Since the pore walls consist of four PPy layers in the thickness direction, two surface layers are available for metal complexation; therefore the Ru/PPy and Ir/PPy ratios for the surface PPy groups were 0.2 and 0.04, respectively.

Computer generated images of Ru-PPy-PMO, based on the assumption of Ru/PPy = 0.2 for the surface PPy and a homogeneous distribution of the Ru complex on the pore surface, are shown in **Fig. 6**. The images clearly indicate that the Ru complex densely accumulated on the surfaces without blocking the pores or disturbing the diffusion of guest molecules in the channels. This structural model suggests that PPy-PMO has the great advantage of retaining its mesoscale pore space, even when metal complexes are integrated onto the pore surfaces (Figs. 6(A) and (B)).

Light harvesting properties were observed in the luminescence spectra of Ir-PPy-PMO (Fig. 5(D)). The emission of Ir-PPy-PMO at 550 nm was greater for an excitation wavelength of 300 nm than 380 nm, suggesting that the 300-nm light energy absorbed by the many PPy groups in the PMO framework is transferred to the relatively few Ir complexes through Förster resonance energy transfer. Although a 420 nm emission from PPy-PMO was observed before cyclometalation, the emission band almost disappeared for Ir-PPy-PMO, suggesting efficient energy transfer from the PPy groups to the Ir complexes on the pore surfaces (Figs. 5(D) and 6(C)).

2. 3 BPy-PMO

We accomplished the first synthesis of a BPy-bridged alkoxysilane precursor that was directly alkoxysilylated at the 5,5'-position of 2,2'-bipyridine and the successful preparation of a novel PMO bearing BPy from a 100% BPy-bridged organosilane precursor (**Scheme 4**). The formation of a periodic mesostructured and a crystal-like arrangement of BPy groups in the pore wall of the BPy-PMO was confirmed by XRD, nitrogen adsorption/desorption properties, TEM, solid state NMR, and IR measurements.[20]

The BPy groups of the PMO functioned as solid chelating ligands. A variety of metal complexes were efficiently formed by stirring a mixture of metal complex precursors and BPy-PMO powder in a solution. The metal complexes prepared from BPy-PMO are summarized in **Fig. 7**. Typical photoredox catalysts, $[Ru(bpy)_3]^{2+}$ and $[Ir(bpy)(ppy)_2]^{+}$, were successfully formed with BPy groups on the pore surfaces. The resulting materials, denoted as Ru-BPy-PMO and Ir-BPy-PMO, respectively, were analyzed by UV/Vis absorption, photoluminescence, and X-ray absorption fine structure (XAFS) measurements.[20] Ir(cod)(OMe)-BPy-PMO was synthesized by mixing BPy-PMO with $[Ir(cod)(OMe)]_2$ in benzene. The coordination structure was investigated by XAFS and X-ray photoelectron spectroscopy (XPS) measurements.[20] Re tricarbonyl complexes, which are well-known two-electron-reduction photocatalysts of CO_2 to CO, were successfully formed in BPy-PMO. In IR spectra of the Re-BPy-PMO, characteristic bands due to CO stretching were observed at 1894

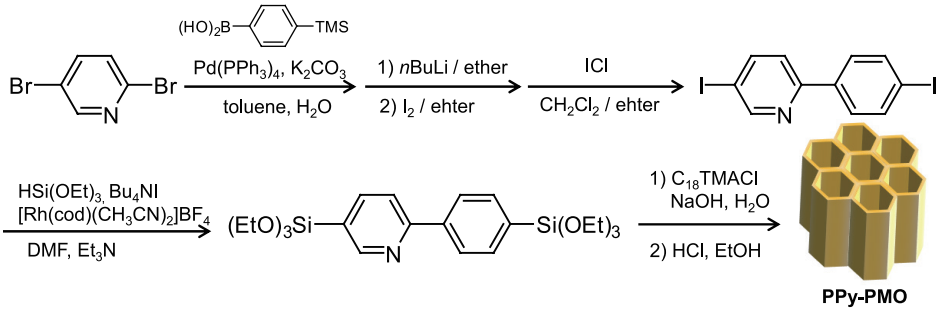

Scheme 3 Synthesis of the PPy precursor and preparation of PPy-PMO.

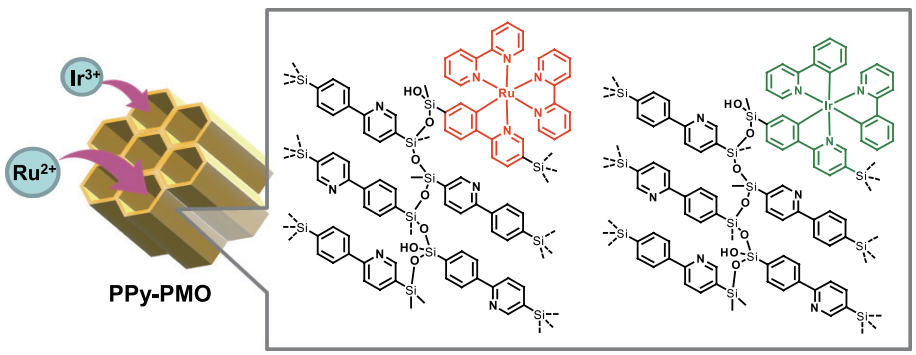

Fig. 4 Formation of Ru and Ir complexes on PPy-PMO.

and 2025 cm^{-1}, in good agreement with those for the model complex, $Re(bpy)(CO)_3Cl$.[20] The formation of Pd-BPy-PMO was confirmed by XPS. Pd-BPy-PMO had a lower binding energy of Pd $3d_{5/2}$ (337.0 eV) than that of $Pd(OAc)_2$ (337.5 eV), indicating that the strong coordination of Pd^{II} species with the electron donating BPy ligand induced a negative shift in the binding energy.[20]

These functional metal complexes were successfully formed in the channels, maintaining the periodicity of the mesostructure and the molecular ordering during complex formation on the pore surfaces. The efficient coordination of metal ions can be attributed to a high degree of freedom of the BPy groups to rotate about the Si-C axis in the crystal-like pore walls. Since the pore walls of BPy-PMO are composed of four BPy layers, only the outermost two surface layers of the BPy are available for complexation. The unique environment of the highly ordered aligned BPy groups causes a dense accumulation of metal complexes on the pore surfaces, resulting in little pore blockage that would hinder the diffusion of molecules and ions in the mesochannels and restrict the catalytic reaction.

We carried out the C-H borylation using Ir(cod)(OMe)-BPy-PMO as a solid catalyst (**Fig. 8**). Direct C-H borylation of benzene gave the desired product in good yield (94%) under the following conditions: PMO catalyst (0.75 mol% Ir), arenes (20 mmol), and bis(pinacolate)diboron (B_2pin_2) (0.33 mmol) at 80°C for 12 h. The yield was higher than in the case of a homogenous Ir catalyst (80%). The other comparable solid materials: Ir-grafted silica gel (33%), mesoporous silica (63%), and polystyrene (no activity), had lower catalytic activities than Ir(cod)(OMe)-BPy-PMO. The PMO catalyst was easily removed and recovered from the reaction mixture, which is a great advantage for a heterogeneous catalyst. The recovered Ir(cod)(OMe)-BPy-PMO exhibited reusability, with good to moderate catalytic activity (94-88%) for at least three cycles.

We demonstrated the construction of a photocatalytic hydrogen evolution system using Ru-BPy-PMO as

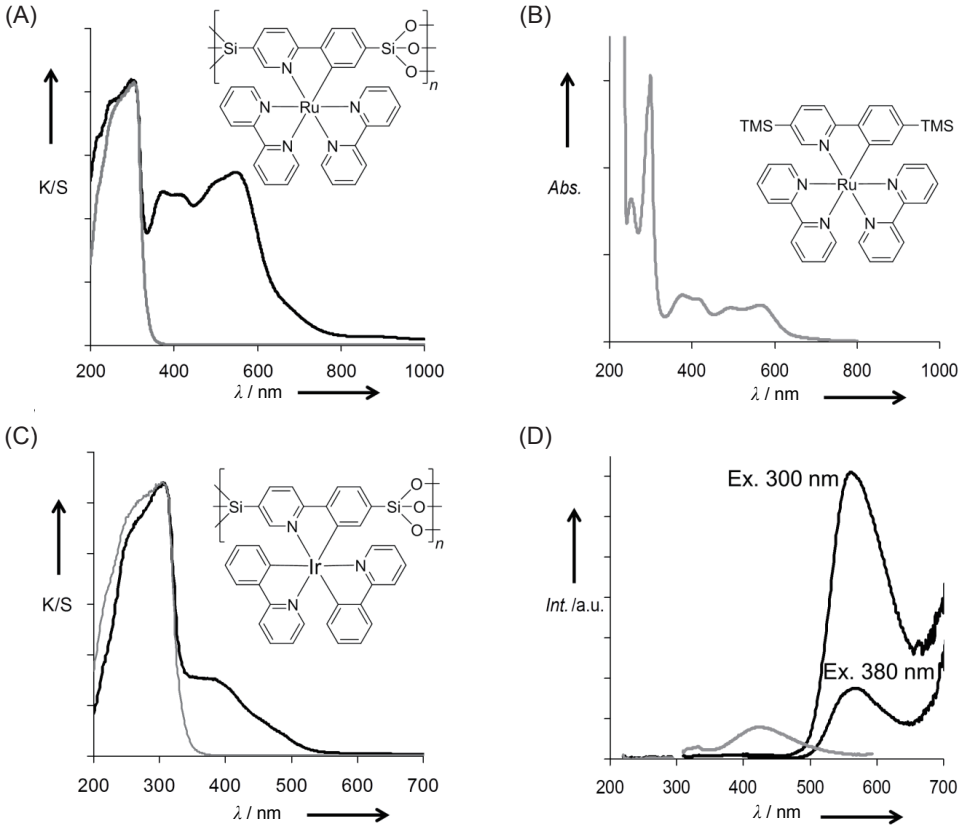

Fig. 5 (A) UV/Vis diffuse reflectance spectra of Ru-PPy-PMO (black) and PPy-PMO (gray). (B) UV/Vis absorption spectrum of the model Ru complex $[Ru(bpy)_2(TMS\text{-}ppy)]^+$ in CH_2Cl_2 (1.0×10^{-5} M). (C) UV/Vis diffuse reflectance spectra of Ir-PPy-PMO (black) and PPy-PMO (gray). (D) Photoluminescence spectra of Ir-PPy-PMO (black) excited at 300 and 380 nm (black) and PPy-PMO excited at 300 nm (gray).

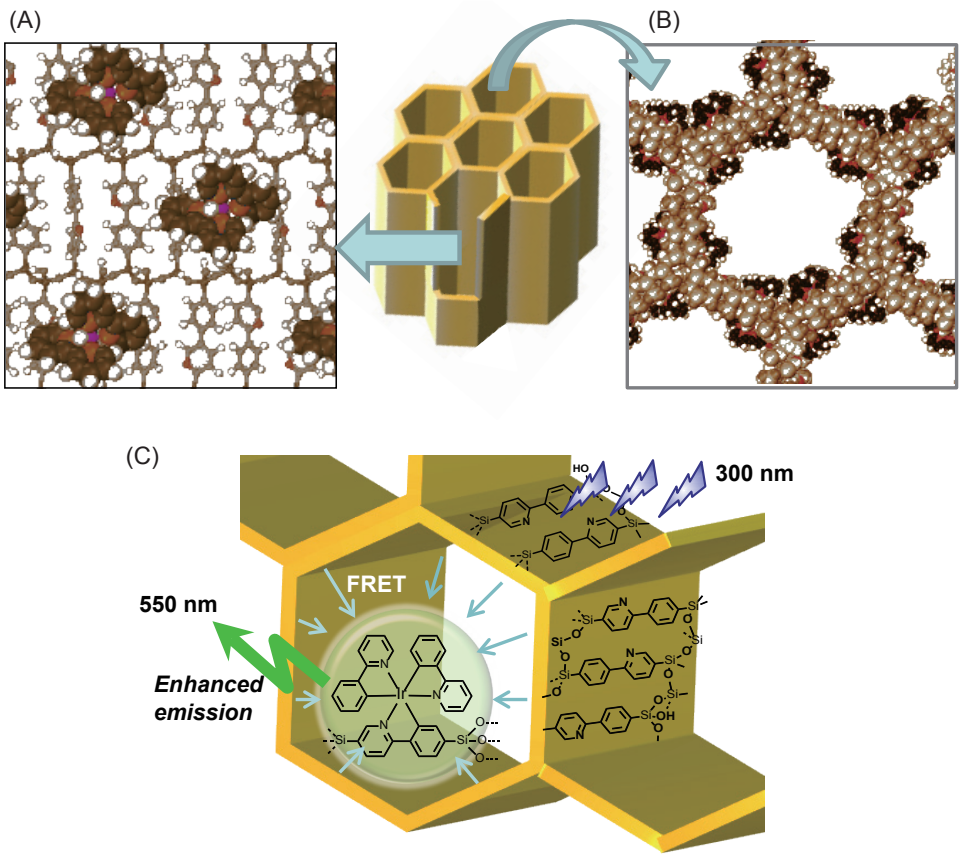

Fig. 6 Computer generated images of (A) Ru complexes on the pore surfaced and (B) a cross section of a mesochannel in Ru-PPy-PMO. (C) A schematic image of light harvesting by Ir-PPy-PMO.

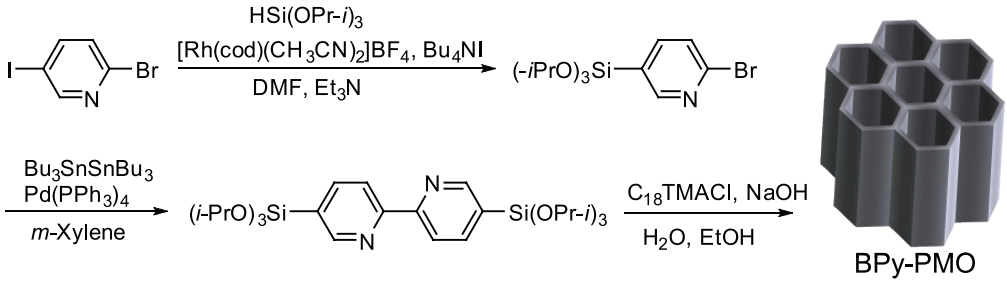

Scheme 4 Synthesis of a BPy-bridged alkoxysilane as a PMO precursor, and the preparation of BPy-PMO.

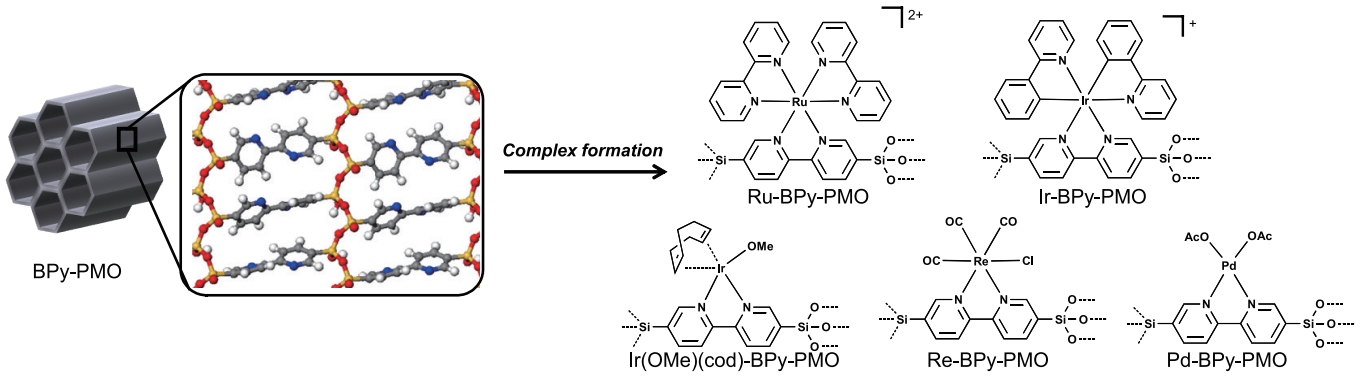

Fig. 7 Complex formation on the pore surface of BPy-PMO (cod: 1,5-cyclooctadiene).

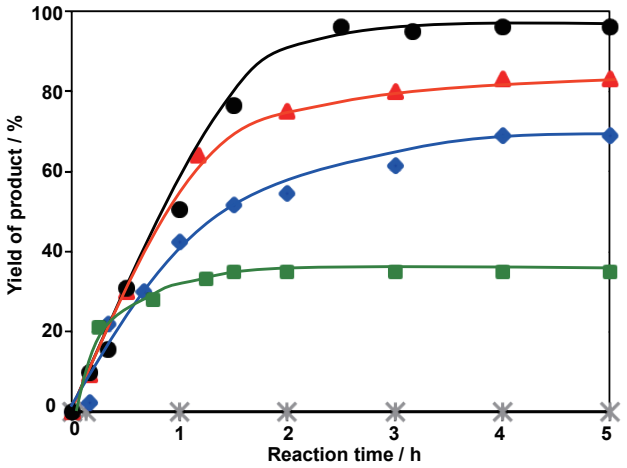

Fig. 8 C-H borylation of benzene using Ir(cod)(OMe)-BPy-PMO (black), homogenous catalyst Ir(cod)(OMe)(bpy) (red), Ir complex grafted on silica gel (blue), Ir complex grafted mesoporous silica (green), and Ir complex grafted polystyrene (gray).

a photosensitizer. Ru-BPy-PMO was loaded with Pt particles by adding Pt^{II} salts in an ethanol solution. Backscattered electron microscopy and dark-field scanning transmission electron microscopy of Pt/Ru-BPy-PMO revealed that the Pt particles were homogeneously loaded into the mesochannels of Ru-BPy-PMO (**Fig. 9**). The photocatalysis test was carried out using a glass-enclosed gas circulation and evacuation system (**Fig. 10**(A)). The vessel was loaded with Ru-BPy-PMO suspended in acetate buffer solution containing EDTA, and then irradiated with visible light (> 385 nm) using a high-power xenon lamp. The produced hydrogen was detected using gas chromatography. As shown in Fig. 10(B), hydrogen was continuously generated under photoirradiation. The Ru-based turnover number reached 184 after 24 h. A photocatalytic hydrogen evolution system based on Ru-BPy-PMO with Pt particles is schematically illustrated in Fig. 10(C). Photoirradiation induces an electron transfer from the photoexcited Ru complex to Pt nanoparticles on the surface of BPy-PMO. Hydrogen is evolved on the Pt particles from protons, while EDTA acts as a sacrificial reagent, returning the Ru complex on the BPy-PMO to its original state.

3. Conclusion

We synthesized novel crystal-like PMOs with three types of pyridyl groups (divinylpyridine, phenylpyridine, and bipyridine) in the framework. These PMOs acted as efficient metal ligands for complex formation on the organic part of the pore surfaces. The successful coordination of metal ions in pyridyl-ligand-bridged PMOs demonstrates their great potential for various applications such as metal adsorbents and heterogeneous catalysts.

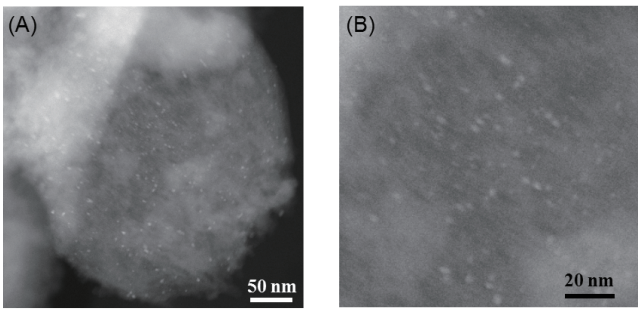

Fig. 9 Backscattered electron microscopy and dark-field scanning transmission electron microscopy images of Pt/Ru-BPy-PMO.

References

(1) Inagaki, S., Guan, S., Fukushima, Y., Ohsuna, T. and Terasaki, O., *J. Am. Chem. Soc*., Vol. 121, No. 41 (1999), pp. 9611-9614.
(2) Asefa, T., MacLachlan, M., Coombs, N. and Ozin, G. A., *Nature*, Vol. 402, No. 6764 (1999), pp. 867-871.
(3) Melde, B. J., Holland, B. T., Blanford, C. F. and Stein, A., *Chem. Mater*., Vol. 11, No. 11 (1999), pp. 3302-3308.
(4) Hunks, W. J. and Ozin, G. A., *J. Mater. Chem*., Vol. 15, No. 35-36 (2005), pp. 3716-3724.
(5) Hoffmann, F., Cornelius, M., Morell, J. and Fröba, M., *Angew. Chem. Int. Ed*., Vol. 45, No. 20 (2006), pp. 3216-3251.
(6) Fujita, S. and Inagaki, S., *Chem. Mater*., Vol. 20, No. 3 (2008), pp. 891-908.
(7) Inagaki, S., Guan, S., Ohsuna, T. and Terasaki, O., *Nature*, Vol. 415, No. 6869 (2002), pp. 304-307.
(8) Kapoor, K. P., Yang, Q. and Inagaki, S., *J. Am. Chem. Soc*., Vol. 124, No. 51 (2002), pp. 15176-15177.
(9) Xia, Y., Wang, W. and Mokaya, R., *J. Am. Chem. Soc*., Vol. 127, No. 2 (2005), pp. 790-798.
(10) Sayari, A. and Wang, W., *J. Am. Chem. Soc*., Vol. 127, No. 35 (2005), pp. 12194-12195.
(11) Cornelius, M., Hoffmann, F. and Fröba, M., *Chem. Mater*., Vol. 17, No. 26 (2005), pp. 6674-6678.
(12) Mizoshita, N., Goto, Y., Kapoor, M. P., Shimada, T., Tani, T. and Inagaki, S., *Chem. Eur. J*., Vol. 15, No. 1 (2009), pp. 219-226.
(13) Wang, W., Lofgreen, J. E. and Ozin, G. A., *Small*, Vol. 6, No. 23 (2010), pp. 2634-2642.

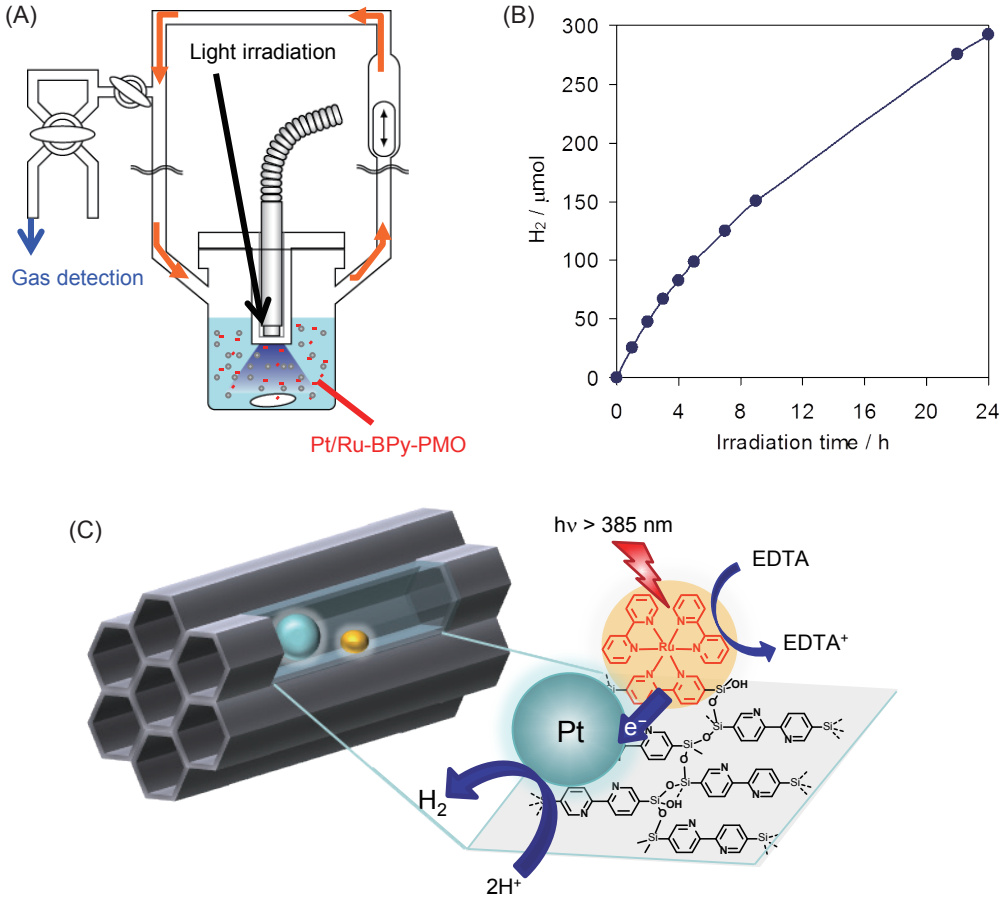

Fig. 10 (A) An illustration of a glass-enclosed gas circulation and evacuation system for photocatalyst evaluation. (B) Hydrogen evolution from Pt/Ru-BPy-PMO under visible light irradiation. (C) A schematic of a photocatalytic hydrogen evolution system based on Pt/Ru-BPy-PMO.

(14) Mizoshita, N., Tani, T. and Inagaki, S., *Chem. Soc. Rev.*, Vol. 40, No. 2 (2011), pp. 789-800.
(15) Burleigh, M. C., Markowitz, M. A., Spector, M. S. and Gaber, B. P., *J. Phys. Chem. B*, Vol. 105, No. 41 (2001), pp. 9935-9942.
(16) Corriu, R. J. P., Lancelle-Beltran, E., Mehdi, A., Reyé, C., Brandès, S. and Guilard, R., *J. Mater. Chem.*, Vol. 12, No. 5 (2002), pp. 1355-1362.
(17) Chen, H.-T., Huh, S., Wiench, J. W., Pruski, M. and Lin, V. S.-Y., *J. Am. Chem. Soc.*, Vol. 127, No. 38 (2005), pp. 13305-13311.
(18) Waki, M., Mizoshita, N., Ohsuna, T., Tani, T. and Inagaki, S., *Chem. Commun.*, Vol. 46, No. 43 (2010), pp. 8163-8165.
(19) Waki, M., Mizoshita, N., Tani, T. and Inagaki, S., *Angew. Chem. Int. Ed.*, Vol. 50, No. 49 (2011), pp. 11667-11671.
(20) Waki, M., Maegawa, Y., Hara, K., Goto, Y., Shirai, S., Yamada, Y., Mizoshita, N., Tani, T., Chun, W.-J., Muratsugu, S., Tada, M., Fukuoka, A. and Inagaki, S., *J. Am. Chem. Soc.*, Vol. 136, No. 10 (2014), pp. 4003-4011.
(21) Manoso, A. S. and Deshong, P., *J. Org. Chem.*, Vol. 66, No. 22 (2001), pp. 7449-7455.
(22) Murata, M., Ishikura, M., Nagata, M., Watanabe, S. and Masuda, Y., *Org. Lett.*, Vol. 4, No. 11 (2002), pp. 1843-1845.
(23) Baldo, M. A., Lamansky, S., Burrows, P. E., Thompson, M. E. and Forrest, S. R., *Appl. Phys. Lett.*, Vol. 75, No. 1 (1999), pp. 4-6.
(24) Baldo, M. A., Thompson, M. E. and Forrest, S. R., *Nature*, Vol. 403, No. 6771 (2000), pp. 750-753.
(25) Kalyanasundaram, K. and Grätzel, M., *Coord. Chem. Rev.*, Vol. 177 (1998), pp. 347-414.
(26) Juris, A., Balzani, V., Barigelletti, F., Campagna, S., Belser, P. and Zelewsky, A. V., *Coord. Chem. Rev.*, Vol. 84 (1988), pp. 85-277.
(27) Nicewicz, D. A. and MacMillan, D. W. C., *Science*, Vol. 322, No. 5898 (2008), pp. 77-80.
(28) Bruce, M. I., *Angew. Chem. Int. Ed.*, Vol. 16, No. 2 (1977), pp. 73-86.
(29) Albrecht, M., *Chem. Rev.*, Vol. 110, No. 2 (2010), pp. 576-623.
(30) Hay, P. J., *J. Phys. Chem. A*, Vol. 106, No. 8 (2002), pp. 1634-1641.

Fig. 5
Reprinted from Angew. Chem. Int. Ed., Vol. 50, No. 49 (2011), pp. 11667-11671, Waki, M., Mizoshita, N., Tani, T. and Inagaki, S., "Periodic Mesoporous Organosilica Derivatives Bearing a High Density of Metal Complexes on Pore Surfaces", © 2011 John Wiley & Sons, Inc., with permission from John Wiley & Sons, Inc.

Minoru Waki
Research Field:
- Synthesis and Functionalization of Periodic Mesoporous Organosilicas

Academic Degree: Ph.D
Academic Societies:
-The Chemical Society of Japan
-The Pharmaceutical Society of Japan
-Japan Association of Zeolite

Yoshifumi Maegawa
Research Fields:
- Organic Synthesis for Functional Organosilica Hybrids
- Synthesis and Catalytic Application of Periodic Mesoporous Organosilicas

Academic Societies:
-The Chemical Society of Japan
-The Society of Synthetic Organic Chemistry, Japan

Norihiro Mizoshita
Research Field:
- Synthesis and Functionalization of Organosilica Hybrid Materials

Academic Degree: Ph.D
Academic Societies:
- The Chemical Society of Japan
- The Society of Polymer Science, Japan
- Japanese Liquid Crystal Society

Awards:
- Japanese Liquid Crystal Society Paper Award (A), 2000
- Young Scientist Award of Japanese Liquid Crystal Society, 2006

Takao Tani
Research Fields:
- Functionalization of Periodic Mesoporous Organosilicas
- Flame Synthesis of Metal Oxide Nanoparticles and Their Applications

Academic Degree: Dr.sc.techn.ETH
Academic Society:
- The Ceramic Society of Japan

Award:
- 40th Tokai Chemical Industry Association Award, 2005

Shinji Inagaki
Research Field:
- Synthesis and Applications of Mesoporous Materials

Academic Degree: Dr.Eng.
Academic Societies:
- The Chemical Society of Japan
- Catalysis Society of Japan
- Japan Association of Zeolite
- The Japan Society on Adsorption
- The Society of Polymer Science, Japan
- International Mesostructured Materials Association
- International Zeolite Association

Awards:
- The Award of Chemistry on Catalyst Preparation, 1994
- The Promotion Award of the Japan Society on Adsorption, 2000
- The Chemical Society of Japan Award for Creative Work, 2004
- The Minister Award of Education, Culture, Sport, Science and Technology, 2005
- The Japan Society on Adsorption Award, 2008

